Sensors and Actuators B 255 (2018) 1173–1181

Contents lists available at ScienceDirect

Sensors and Actuators B: Chemical

journal homepage: www.elsevier.com/locate/snb

Research Paper

Mixed potential type sensor based on stabilized zirconia and $Co_{1-x}Zn_xFe_2O_4$ sensing electrode for detection of acetone

Xidong Hao[b], Bin Wang[b], Ce Ma[b], Fangmeng Liu[b], Xue Yang[b], Tong Liu[b], Xishuang Liang[a,b,*], Chunhua Yang[c], Hongqiu Zhu[c], Geyu Lu[a,b,*]

[a] State Key Laboratory of Automotive Simulation and Control, Jilin University,5988 Renmin Avenue, Changchun 130012, China
[b] State Key Laboratory on Integrated Optoelectronics, College of Electronic Science and Engineering, Jilin University,2699 Qianjin Street, Changchun 130012, China
[c] School of Information Science and Engineering, Central South University, Changsha 410083, China

ARTICLE INFO

Article history:
Received 6 March 2017
Received in revised form 22 May 2017
Accepted 1 June 2017
Available online 2 June 2017

Keywords:
Acetone sensor
Stabilized zirconia
$Co_{1-x}Zn_xFe_2O_4$
Mixed-potential

ABSTRACT

A series of spinel oxides $Co_{1-x}Zn_xFe_2O_4$ (x = 0, 0.3, 0.5, 0.7 and 1) prepared by a facile sol-gel method were used as sensing electrodes of mixed potential type yttria stabilized-zirconia (YSZ)-based gas sensor for detection of acetone. The present study mainly focused on the influence of different proportions of cobalt and zinc in $Co_{1-x}Zn_xFe_2O_4$ –sensing electrode (SE) on the acetone sensing properties for the sensor, and the results showed that when x = 0.5, the fabricated sensor exhibited a largest sensitivity of −63 mV/decade to 5–100 ppm acetone at 650 °C. The response signal of the present sensor to 50 ppm acetone was as large as −112 mV, and even could achieve low detection limit of 300 ppb at 650 °C, which had a faithful response at this concentration. In addition, the present device also displayed good reliability, good cross sensitivities in the presence of various interfering gases, slight sensitive effect to humidity and good stability over 40 days at 650 °C. Moreover, the polarization curve was measured to further demonstrate the mixed potential mechanism.

1. Introduction

Acetone, as known as a dimethyl ketone, is the simplest saturated ketone with colorless transparent liquid and special spicy smell. Inhaling acetone will cause serious adverse reactions and even poisoning, acute intoxication will have a narcotic effect on the central nervous and appear some symptoms, such as fatigue, dizziness, nausea and easy excited. Inhaling acetone severely can lead to vomiting, cramps, and even coma. Long-term inhaled acetone can also cause dermatitis [1–3]. So, the detection of acetone is very important in public. At the same time, with the improvement of people's living standard, the number of people with diabetes is increasing day by day. Exhale and clinical medicine show that the acetone gas concentration in exhaled breath of patients with diabetes expired was more than 1.8 parts per million, far higher than normal person with 0.3–0.9 ppm [4–6]. Therefore, by developing portable instrument and real-time monitoring acetone concentration in the exhaled breath of suspected patients, it is conducive to the prevention and early diagnosis of diabetes.

Nowadays, the detection of low concentration of gas mainly relies on large-scale analysis instruments, such as gas chromatography/mass spectroscopy (GC/MS) and differential mobility spectroscopy (DMS) [7], however, these methods have some disadvantages of large size, high price and disability to real-time detection, which limit the application in diagnosis of diabetes [8,9]. Gas sensor with low price, simple fabrication, high sensitivity, which is able to detect in real time and build a portable gas detector, is becoming one of the most written topics. In recent years, solid state electrochemical gas sensor based on the solid electrolyte and composite oxide sensing electrodes because of its high sensitivity, fast response and good selectivity has been widely investigated.

At present, among the various gas sensors reported [10–18], mixed potential type gas sensors utilizing yttria-stabilized zirconia (YSZ) as solid electrolyte and metal oxide sensing electrode were designed and investigated in a wide application. For mixed potential type gas sensor, the category of sensing electrode material is vital to the improve sensing performance of the sensor. Some typical simple and sensing electrodes materials were widely developed by some groups to fabricated VOC sensor and resulted in good sensing characteristics, like SnO_2, WO_3, Sm_2O_3, $Zn_3V_2O_8$ and $NiNb_2O_6$

* Corresponding authors at: State Key Laboratory of Automotive Simulation and Control, Jilin University,5988 Renmin Avenue, Changchun 130012, China
E-mail addresses: liangxs@jlu.edu.cn (X. Liang), lugy@jlu.edu.cn (G. Lu).

http://dx.doi.org/10.1016/j.snb.2017.06.002
0925-4005/

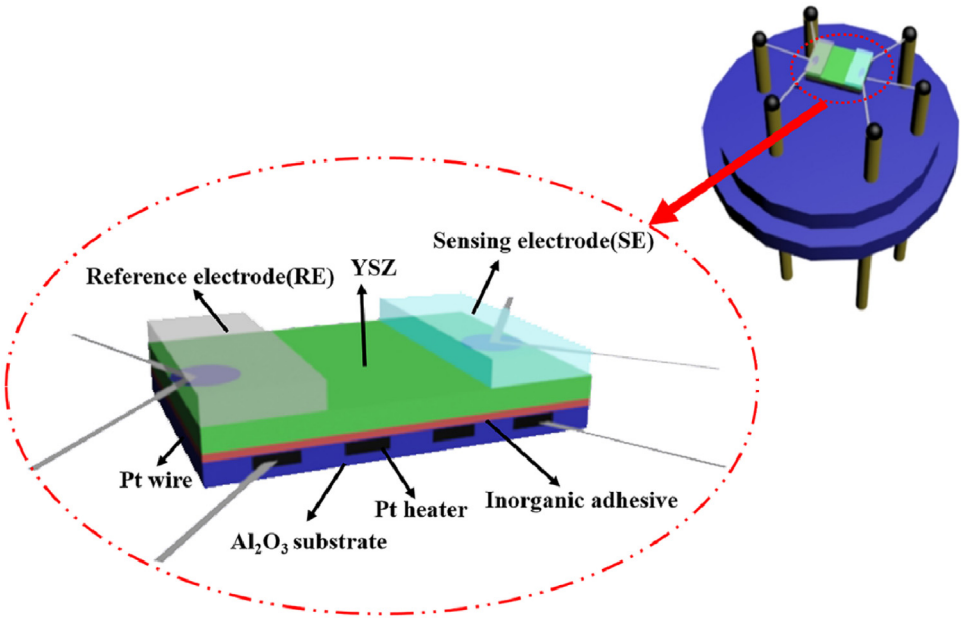

Fig. 1. Structure of the fabricated sensors.

[7,10,16,19,21]. As an important composite oxides, spinel-type oxide were tapped for its potential in electronic and optoelectronic applications [22–24]. Our group synthesized $MnCr_2O_4$ [21] sensing material to fabricate YSZ-based mixed potential type gas sensor and the device displayed perfect sensitive properties to NO_2. As a type of spinel oxide, $ZnFe_2O_4$ has been reported to fabricated mixed potential sensors [25], in addition, Deligoz. H et al. investigated the electrical properties of $Co_{1-x}Zn_xFe_2O_4$ and Rani. R et al. described the AC conductivity properties of nano-crystalline zinc substituted cobalt ferrite synthesized [26,27], however, there is no report about using these materials to fabricated YSZ-based mixed potential type gas sensor. Herein, YSZ-based mixed potential type gas sensor using $Co_{1-x}Zn_xFe_2O_4$ sensing electrode was first developed, aiming at further improving the acetone sensing performance.

Herein, YSZ-based mixed potential type gas sensor using $Co_{1-x}Zn_xFe_2O_4$ sensing electrode was first developed, aiming at further improving the acetone sensing performance. Additionally, the gas sensing properties of the present device to acetone were systematically investigated and the sensing mechanism was discussed.

2. Experimental

2.1. Preparation and characterization of $Co_{1-x}Zn_xFe_2O_4$ sensing electrode material

The $Co_{1-x}Zn_xFe_2O_4$ (x = 0, 0.3, 0.5, 0.7 and 1) were prepared by a sol-gel method. Iron nitrate nonahydrate ($Fe(NO_3)_3{\cdot}9H_2O$), zinc nitrate tetrahydrate ($Zn(NO_3)_2{\cdot}4H_2O$), cobalt nitrate hexahydrate ($Co(NO_3)_2{\cdot}4H_2O$) and citric acid (CA) purchased from Sinopharm Chemical Reagent Co., Ltd were used as raw materials and all of materials were of analytic grade without further purification. First of all, Stoichiometric quantities of metal nitrates were dissolved in deionized water to prepare nitrate solutions, respectively. Next, the zinc nitrate solution and cobalt nitrate solution were drop wise into the ferric nitrate solution, the mixed solution were stirring in the water bath at 60 °C to form precursor solution. Then, citric acid with the mole proportion of citric acid and metal iron = 1:1 was drop into the mixed solution. The mixed solution was stirred at 80 °C for two hours until a gel was obtained. Then, the resultant gel was maintained at 80 °C for 24 h at a vacuum drying oven. Finally, the precursor gel was introduced into a muffle furnace and sintered at 800 °C for 2 h to get target products.

The XRD patterns of the samples were identified by Rigaku wide-angle X-ray diffractometer (D/max rA, using Cu Kα radiation at wave length = 0.1541 nm) in the angular range of 2θ = 20–80°. The surface morphology and micro-structure were investigated using a field-emission scanning electron microscope (FE-SEM, JEOL JSM-7500F) operating at 15 kV.

2.2. Fabrication and measurement of gas sensor

The structure of the sensor we fabricated is shown in Fig. 1, the sensor was manufactured using YSZ plate (8mol% Y_2O_3-doped, 2mm × 2 mm square, 0.3 mm thickness, provided by Anpeisheng Corp. China). A point-shaped and a narrow stripe-shaped Pt electrode (reference electrode, RE) were formed on two ends of the YSZ plate using a commercial Pt paste (Sino-platinum Metals Co. Ltd.), and sintered at 950 °C. The paste which was mixed by a minimum quantity of deionized water and the various sensing materials ($Co_{1-x}Zn_xFe_2O_4$ (x = 0, 0.3, 0.5, 0.7 and 1)). Next, the resultant paste was applied on the point-shade Pt to form stripe-shaped sensing electrode (SE). Afterward, the device was annealed at 800 °C to make a good contact between the sensing electrode and electrolyte. The Pt heater printed on Al_2O_3 substrate was the fixed to the YSZ plate by the inorganic adhesive, which provided the required heating temperature for the sensor.

The gas sensing properties of the sensors we fabricated were tested by a conventional static method. The Pt heater provided enough heat in order to satisfy the right temperature to the sensors with a linear DC Power Supply (Gwinstek GPD-3303S) providing a stable current and the device was put in airtight chamber with volume of 1L when measuring, the pure air was filled using an air pump, and then the number of sample gas was injected into the chamber. When the sensors exposed to air or sample gas, it has a series of voltage signals because of the difference of the electric potential between the SE and RE. A digital electrometer (Rigol Technologies, Inc, DM3058, China) was used to accept and deal with the signals. The results we obtained were recorded with a computer connected to the electrometer. The desired concentration of the sample gas was obtained by the static liquid gas distri-

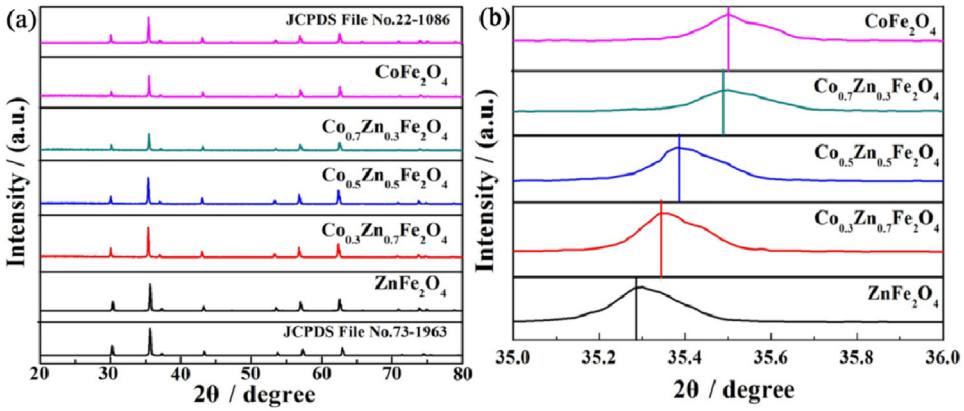

Fig. 2. (a) XRD patterns of $Co_{1-x}Zn_xFe_2O_4$ (x = 0, 0.3, 0.5, 0.7 and 1) composite oxide materials sintered at 800 °C. (b) amplified XRD patterns of $Co_{1-x}Zn_xFe_2O_4$ (x = 0, 0.3, 0.5, 0.7, 1) composite oxide materials at (311) crystal face.

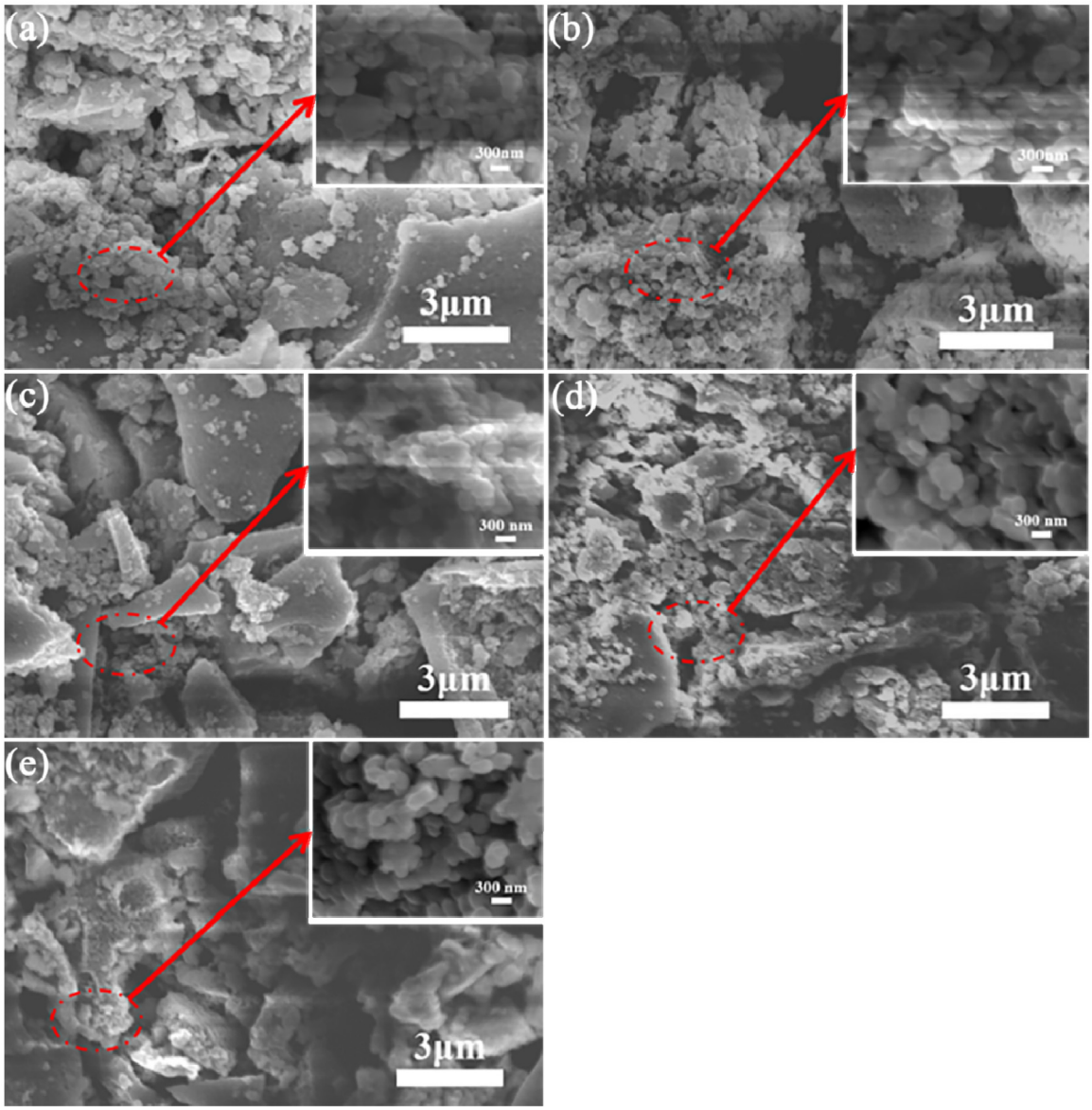

Fig. 3. SEM images of $Co_{1-x}Zn_xFe_2O_4$ (x = 0, 0.3, 0.5, 0.7 and 1)-SEs sintered at 800 °C. (a) $CoFe_2O_4$; (b) $Co_{0.7}Zn_{0.3}Fe_2O_4$; (c) $Co_{0.5}Zn_{0.5}Fe_2O_4$; (d) $Co_{0.3}Zn_{0.7}Fe_2O_4$; (e) $CoFe_2O_4$.

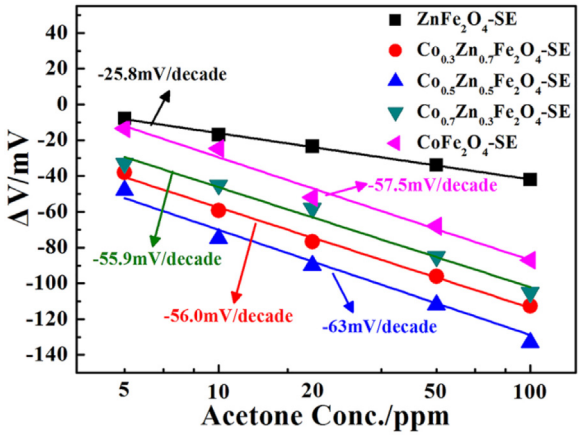

Fig. 4. Dependence of Δ V on the logarithm of acetone concentrations for the sensors utilizing $Co_{1-x}Zn_xFe_2O_4$ (x = 0, 0.3, 0.5, 0.7 and 1)-SEs in the concentration range of 5–100 ppm acetone at 650 °C.

bution method, which was calculated by the following formula [7,21,28–30].

$$C = \frac{22.4 \times \rho \times \varphi \times V_1}{M \times V_2} \times 100$$

In this formula, the C (ppm) meant the desired concentration of the sample gas; ρ (g/mL) the density of the liquid; φ the required gas volume fraction; V_1 (L) and V_2 (L) the volume of the liquid and chamber, respectively; and M (g/mol) the molecular weight of the liquid. The current–voltage (polarization) curves of the sensor were carried out via the potential dynamic method (CHI650C, Instrument corporation of Shanghai, China) using a two-electrode configuration in the base gas (air) and the different concentrations of acetone gas.

3. Result and discussion

The X-ray diffraction (XRD) was used to identify the crystallographic structure and crystallinity of the as-synthesized $Co_{1-x}Zn_xFe_2O_4$ (x = 0, 0.3, 0.5, 0.7 and 1) products and the results are shown in Fig. 2(a). It can be seen that $CoFe_2O_4$ and $ZnFe_2O_4$ retain their crystallographic phases corresponding to JCPDS File No.22-1086 and JCPDS File No.73-1963, respectively, and are testified to be spinel-type oxides. Moreover, the as-prepared oxides ($Co_{1-x}Zn_xFe_2O_4$) retain their crystallographic phases corresponding to JCPDS File No.73-1963 and also perform a spinel-type structure. With the increase of the amount of cobalt in $Co_{1-x}Zn_xFe_2O_4$, due to the fact that the radius of Zn ions (0.82 Å) is larger than that of the Co ions (0.78 Å), addition of Zn at the expense of Co in the ferrite is expected to increase the lattice constant and

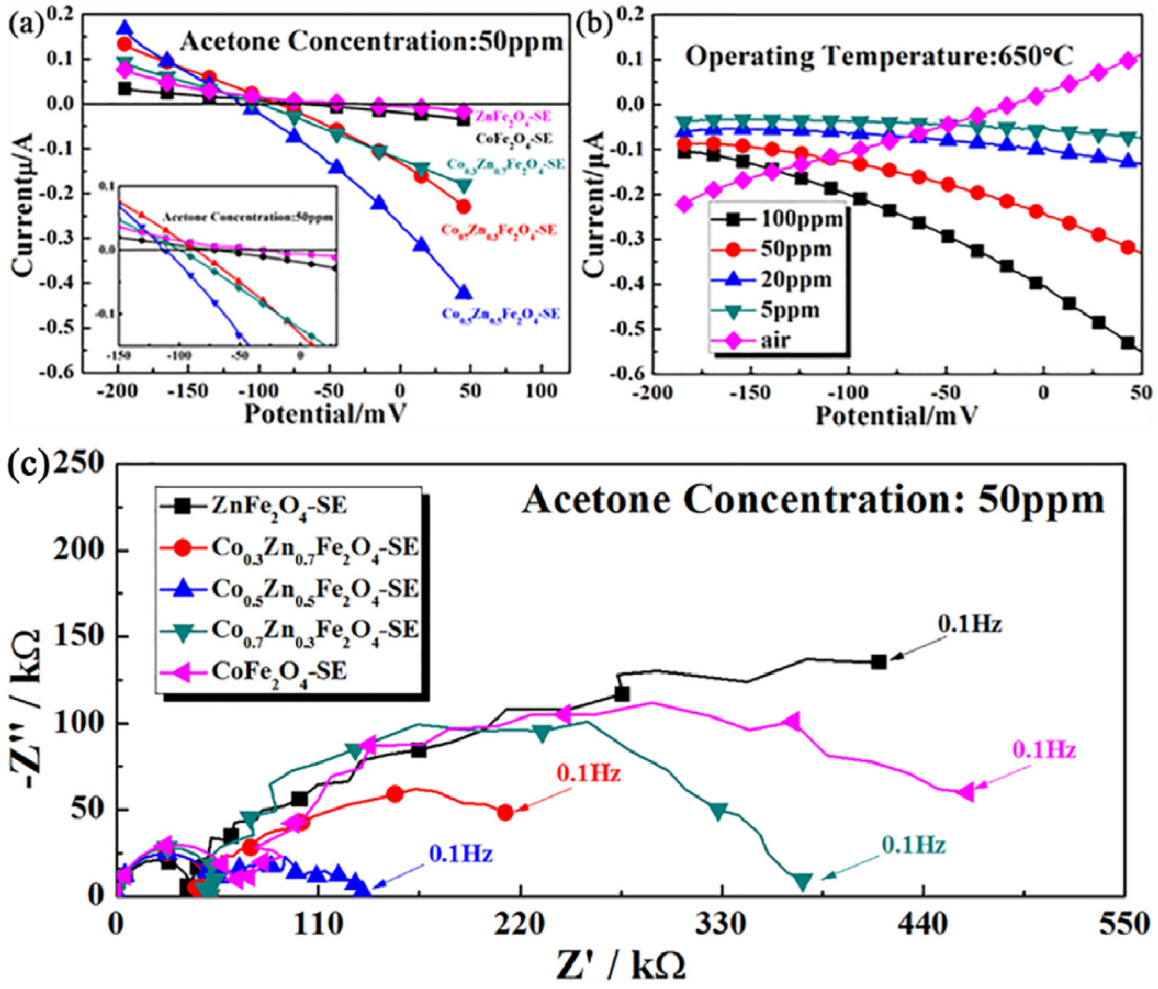

Fig. 5. (a) Polarization curves in sample gas of air and 50 ppm acetone for the sensors using $Co_{1-x}Zn_xFe_2O_4$ (x = 0, 0.3, 0.5, 0.7 and 1)-SEs at 650 °C. (b) Polarization curves in different concentrations of acetone and air for the sensor using $Co_{0.5}Zn_{0.5}Fe_2O_4$-SE at 650 °C. (c) Complex impedance curves in 50 ppm acetone for the sensors attached with $Co_{1-x}Zn_xFe_2O_4$ (x = 0, 0.3, 0.5, 0.7 and 1)-SEs.

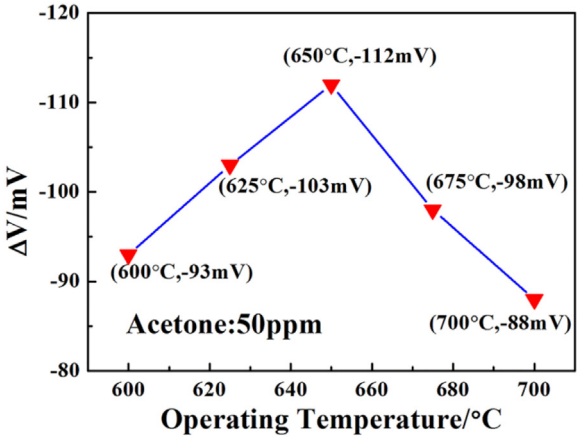

Fig. 6. The response of sensor attached with $Co_{0.5}Zn_{0.5}Fe_2O_4$-SE to 50 ppm acetone at different operating temperatures.

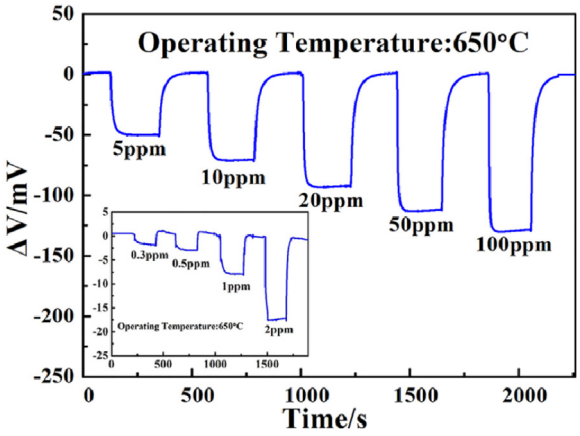

Fig. 7. Response and recovery transient curves for the sensor attached with $Co_{0.5}Zn_{0.5}Fe_2O_4$-SE to different concentrations of acetone in the range of 0.3–100 ppm at 650 °C.

the diffraction peaks shift to the left and the result was shown in Fig. 2(b). In addition, the surface morphology of $Co_{1-x}Zn_xFe_2O_4$ sintered at 800 °C was studied by FESEM and the result is shown in Fig. 3. When the ratio of cobalt and zinc was 1:1, the SE had the largest hole. This porous structure is very important to diffusion of the gas molecular within the material.

For the purpose to explore the influence of the ratios of cobalt and zinc on the acetone sensing properties, the sensors attached with $Co_{1-x}Zn_xFe_2O_4$ (x = 0, 0.3, 0.5, 0.7 and 1)-SE sintered at 800 °C were fabricated and the dependence of ΔV on the logarithm of acetone concentration are exhibited in Fig. 4, it is clear that all of devices displayed a good linear relationship between ΔV and the logarithm of acetone concentration, which conforms to the mixed-potential type sensor [31–33]. Otherwise, the sensor attached with $Co_{0.5}Zn_{0.5}Fe_2O_4$-SE showed the highest response values to every acetone concentration and the largest sensitivity (slope) to acetone in the tested concentration range of 5–100 ppm at 650 °C, compared with those of utilizing other ratios of cobalt and zinc ferrite materials-SE. According to the early work by Co-workers [32,34,35], the sensing characteristics of the present devices abide by the mixed-potential theory and it has the following electrochemical reactions for the sensor.

Inair : O_2, $Co_{1-x}Zn_xFe_2O_4$/YSZ/Pt, O_2

Insamplegas : $C_3H_6O + O_2$, $Co_{1-x}Zn_xFe_2O_4$/YSZ/Pt, $C_3H_6O + O_2$

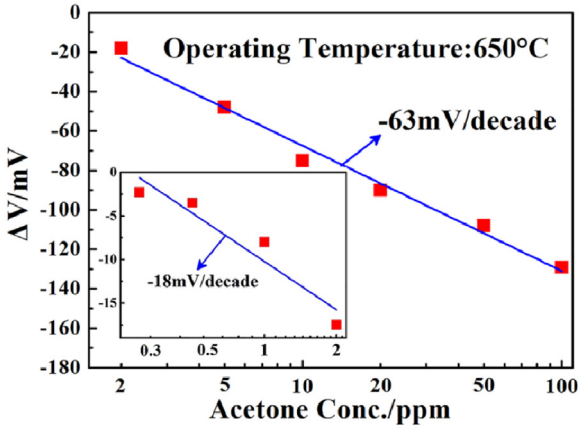

Fig. 8. Dependence of ΔV for the sensor attached with $Co_{0.5}Zn_{0.5}Fe_2O_4$-SE on logarithm of acetone concentration in the range of 0.3–100 ppm at 650 °C.

The electrochemical cathodic (2) and (3) reactions take place at TPB (tripe phase boundary, the interface of $Co_{1-x}Zn_xFe_2O_4$-SE, acetone and YSZ) at the same time when the sensor under the acetone gas atmosphere and form a local cell at SE. When the electrochemical reactions is equal to each other, a dynamic equilibrium reached and the electrode potential is called the mixed potential. The potential difference between the sensing electrode and reference electrode is required and regarded as the sensing signal.

$$C_3H_6O + 4O_2 \rightarrow 3CO_2 + 3H_2O \quad (1)$$

$$4O_2 + 16e^- \rightarrow 8O^{2-} \quad (2)$$

$$C_3H_6O + 8O^{2-} \rightarrow 3CO_2 + 3H_2O + 16e^- \quad (3)$$

As for the sensor we fabricated, the sensing signal relies on the acetone gas concentration took part in the electrochemical reaction at TPB. Therefore, more number of acetone participated in the electrochemical reaction and higher electrochemical reaction action to acetone result in more obvious sensing signals, the micro-structure of $Co_{1-x}Zn_xFe_2O_4$ –SE in Fig. 3 exhibits that the $Co_{1-x}Zn_xFe_2O_4$-SE performed porous structure, which speed up the velocity of gas diffusion to the TPB and shorten the time of reaction (1) in sensing electrode layer. In this case, the acetone consumption caused by oxidation reaction (1) is reduced and more acetone gas reached the TPB directly participate in electrochemical reactions (2) and (3). Furthermore, in order to compare the electrochemical reaction action for the sensors utilizing $Co_{0.5}Zn_{0.5}Fe_2O_4$-SE, the polarization curves in the mixture gas of air and 50 ppm acetone at 650 °C is shown in Fig. 5(a). According to Fig. 5(a), the slope of the polarization curve for the sensor used $Co_{0.5}Zn_{0.5}Fe_2O_4$-SE to 50 ppm acetone is the largest compared with the other sensors, which reveals the sensor attached with $Co_{0.5}Zn_{0.5}Fe_2O_4$-SE has the highest electrochemical catalytic activity [36]. In order to further explain the difference of sensing property for the sensor based on $Co_{1-x}Zn_xFe_2O_4$-SE. The complex impedance was investigated and result is shown in Fig. 5. (c). According to the previous literature [37,38], the total resistance of the sensor affected by the interfacial resistance between the SE and YSZ. The interfacial resistance is given by the resistance value at the intersection of the large semi-arc with the real axis at lower frequencies (around 0.1 Hz). The total impedance includes contributions at low frequency which are typically related to mass transport processes such as gas diffusion and adsorption. Miura et al. reported that the sensitivity of sensor might be attributable to the change in the resistance of electrochemical reaction between the interface of YSZ/oxide SE and sample gas at a high temperature [37–40]. Obviously, the interfacial resistance of the sensor based on $Co_{0.5}Zn_{0.5}Fe_2O_4$-SE was decreased com-

Table 1
Comparison of the mixed potential estimated and the potential difference value observed for the sensors attached with $Co_{1-x}Zn_xFe_2O_4$ (x = 0, 0.3, 0.5, 0.7 and 1)-SEs sintered at 800 °C.

Sensor	Acetone.Conc (ppm)	Mixed potential (estimated) (mV)	Potential difference value (observed) (mV)
$Co_{0.5}Zn_{0.5}Fe_2O_4$-SE	5	−47	−48
$Co_{0.5}Zn_{0.5}Fe_2O_4$-SE	20	−70	−74
$Co_{0.5}Zn_{0.5}Fe_2O_4$-SE	50	−114	−112
$Co_{0.5}Zn_{0.5}Fe_2O_4$-SE	100	−136	−132

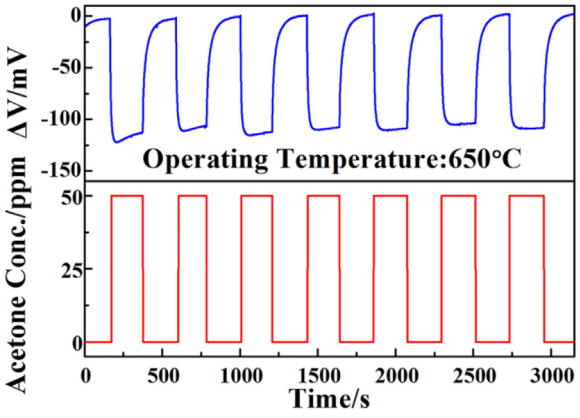

Fig. 9. Continuous response-recovery transient curves to 50 ppm acetone for the sensor using $Co_{0.5}Zn_{0.5}Fe_2O_4$-SE at 650 °C.

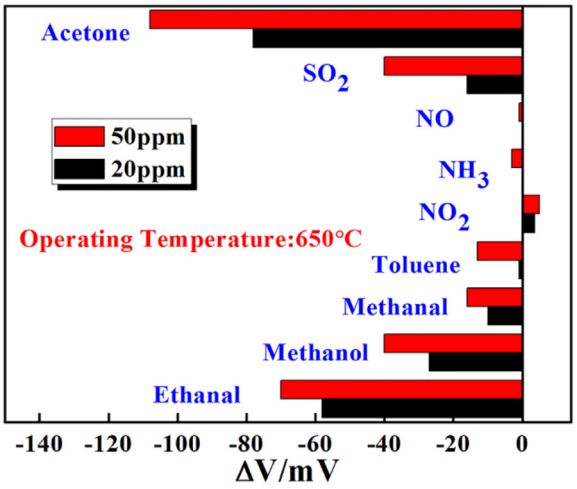

Fig. 10. The cross-sensitivities for the sensor based on $Co_{0.5}Zn_{0.5}Fe_2O_4$-SE to various gases at 650 °C.

pared with other sensors at the lower frequency range. Changes in the interface resistance measured in different sensors mean the ability of electrochemical catalytic activity and the result revealed that $Co_{0.5}Zn_{0.5}Fe_2O_4$-SE performs the highest electrochemical catalytic activity, which was conformed to the sensing properties the sensor based on $Co_{1-x}Zn_xFe_2O_4$-SE performed. Due to the above two points, the sensor attached with $Co_{0.5}Zn_{0.5}Fe_2O_4$-SE has highest sensitivity to acetone. In addition, the polarization curves of the sensor attached with $Co_{0.5}Zn_{0.5}Fe_2O_4$-SE to air and different concentration of the acetone (5 ppm, 20 ppm, 50 ppm, 100 ppm) which were used to better identify the mixed potential theory are exhibited in Fig. 5(b) and the data is shown in Table 1. The cathodic polarization curve was obtained in air, and the anodic polarization curve [36,41,42] was obtained by subtracting in air from in sample gas (different concentrations of acetone + air). The estimated values were in close proximity to those observed values under all circumstances. These coincidences further indicate that the present sensors support the sensing mechanism involving the mixed potential [43–45].

Fig. 6 shows the response ($\Delta V = V_{sampl\ gas} - V_{bas\ gas}$) to 50 ppm acetone of sensor using $Co_{0.5}Zn_{0.5}Fe_2O_4$-SE at different working temperatures (600, 625, 650, 675 and 700 °C). The response to 50 ppm acetone shifted upward as the operating temperature increases from 600 °C to 650 °C, but shifted downward suddenly from 650 °C to 700 °C. The reason was that the reaction on the SE needed much activation energy and when temperature was below 650 °C, the activation energy for the reaction was not enough. Hence, with the increase of the operating temperature, the activation energy increased, which made the sensitivity increased. However, the acetone consumption ($C_3H_6O + 4O_2 \rightarrow 3CO_2 + 3H_2O$) caused by the high chemically catalytic activity of $Co_{0.5}Zn_{0.5}Fe_2O_4$ sensing electrode in the process of acetone diffusion was facilitated at higher working temperature. In addition, when at higher temperature, adsorption is becoming more and more difficult, and stripping easier. As a result, the decreased amount of acetone reached the TPB and participated in the electrochemical reactions along with the increasing working temperature. Consequently, the optimal working temperature for the present sensor was considered to be 650 °C and the sensing characteristics were investigated mainly at present temperature in the next work.

Fig. 7 shows the response transients of sensor attached with $Co_{0.5}Zn_{0.5}Fe_2O_4$-SE annealed to different concentrations of acetone in the range of 0.3–100 ppm. The present device showed fast response and recovery rates to every concentration of acetone. Further, the typical 90% response and recovery times was toward different concentrations of acetone was less than 10 s and the response value of sensor attached with $Co_{0.5}Zn_{0.5}Fe_2O_4$-SE to 50 ppm acetone at 650 °C was about −112 mV. It is worth noting that the low detection limit of the present sensor was 300 ppb and the response value was −2.1 mV, which displayed the ability of low concentration acetone detection. In addition, the relationship between ΔV and the logarithm of acetone concentration for the sensor utilizing $Co_{0.5}Zn_{0.5}Fe_2O_4$-SE is exhibited in Fig. 8. It is obvious that the ΔV and the logarithm of acetone concentration in the both range of 0.3–2 ppm and 2–100 ppm displayed a good linear relationship at 650 °C, which was accorded with mixed potential type model [7,33–35,45]. The sensitivities of the present sensor to acetone were −18 mV/decade in the concentration range of 0.3–2 ppm and −63 mV/decade in the concentration range of 2–100 ppm, respectively. It is widely known that the electrochemical reaction for the present mixed potential type acetone sensor occurred at the TPB and the sensing performance of the sensor is associated with the acetone with the acetone concentration at TPB. When the acetone gas go through the sensing electrode layer, the oxidation reaction (1) of acetone takes place and the sample gas is partly consumed before arriving at TPB. At the high concentration scope of acetone (2–100 ppm), the consumption is insignificant for total acetone concentration due to the good porosity of the sensing electrode. However, at low concentration scope (0.3–2 ppm), the effect of acetone consumption is an important factor and should not be neglected. Hence, the acetone concentration arrived at TPB at

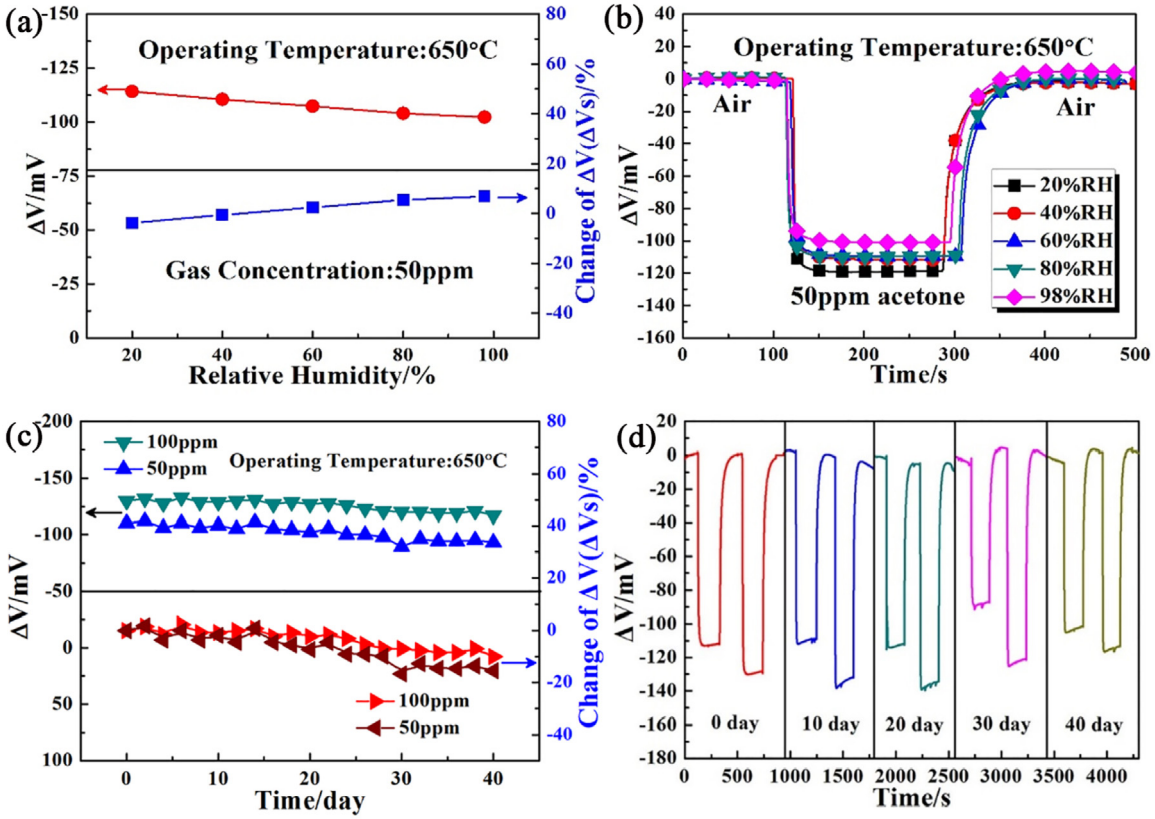

Fig. 11. (a) Response of the sensor attached with $Co_{0.5}Zn_{0.5}Fe_2O_4$-SE to 50 ppm acetone at 650 °C under different relative humidities. (b) Response and recovery transients for the sensor using $Co_{0.5}Zn_{0.5}Fe_2O_4$-SE annealed at to 50 ppm acetone under 20%, 40%, 60%, 80% and 98% RH at 650 °C. (c) Long-term stability for the sensor attached with $Co_{0.5}Zn_{0.5}Fe_2O_4$-SE to 50 and 100 ppm acetone at 650 °C. (d) Response and recovery transients for the sensor using $Co_{0.5}Zn_{0.5}Fe_2O_4$-SE at 650 °C to 50 and 100 ppm acetone on the initial, 10th, 20th, 30th and 40th days at 650 °C.

Table 2
Comparison of the sensing performance of the present sensor and that of devices reported in literatures.

Sensing electrode	Acetone.Conc (ppm)	Response (mV)	Sensitivity (mV/decade)	Low Detection Limit (ppm)	Ref.
$Co_{0.5}Zn_{0.5}Fe_2O_4$	100	−132	−63	0.3	Present work
$NiNb_2O_6$	100	−113	−79	0.5	[7]
$Zn_3V_2O_8$	100	−69	−56	1	[20]
$NiCr_2O_4$	100	−60	−60	–	[46]
SnO2	100	22	45	–	[19]
$Pt/CeO_2/SnO_2$	100	19	36	–	[47]
Porous $ZnO/ZnCo_2O_4$	100	7.5 (R = Ra/Rg)		10	[48]
Flower-like WO_3	100	17.4 (R = Ra/Rg)		1	[49]
Ce-doped SnO_2 hollow spheres	100	12 (R = Ra/Rg)		50	[50]
ZnO nanorod	100	30.4 (R = Ra/Rg)		1	[51]
$ZnFe_2O_4$ hollow microspheres	100	38 (R = Ra/Rg)		1	[52]
$ZnO/ZnFe_2O_4$ nanosheets	100	16.8 (R = Ra/Rg)		5	[53]

low concentration scope reduce greatly compared with that at high concentration scope, which led to a reduction in sensitivity. In addition, on account of the difference of the atmospheric between high and low concentration, the diffusion rate had a vast differences, as shown in following formula:

$$v = \frac{dc}{dt} = D\frac{d^2c}{dx^2} = D\frac{d^2}{dx^2}\left(\frac{p}{RT}\right) = \frac{D}{RT}\frac{d^2p}{dx^2}$$

In this formula, the v (ppm/s) meant the diffusion rate; c (ppm) the desired acetone gas concentration; D the diffusion coefficient; p (kPa) gas pressure between gaseous phase and TPB; x (μm) diffusion length; T (K) operating temperature, respectively; and R (J/mol·K) the gas constant. When D, T and x were constant, between the diffusion rate and the gas pressure displayed a positive correlation relationship, and the gas pressure at low concentration slope was lower than that at high concentration slope, thus, the diffusion rate at low concentration scope was slower. In addition, the faster acetone diffusion rate shortens time went through the sensing electrode layer and acetone consumption was reduced. Therefore, the percentage of acetone gas in lower concentration range arrived at TPB was less than that in higher concentration range. In this case, the present sensor exhibited the lower sensitivity to acetone in the low concentration range (0.3–2 ppm) than that in the high concentration range (2–100 ppm).

The continuous response and recovery characteristic to the certain concentration of acetone for gas sensor is an important sensing performance parameter, and the continuous response and recovery curve of the sensor attached with $Co_{0.5}Zn_{0.5}Fe_2O_4$-SE to 50 ppm acetone at 650 °C is demonstrated in Fig. 9. The response value of the present device exhibited little fluctuation and the highest and lowest change errors of continuous responses, respectively. Additionally, the selectivity was one of the most important sensing

properties for the sensor, and Fig. 10 shows the response signals for the sensor attached with $Co_{0.5}Zn_{0.5}Fe_2O_4$-SE to a series of interfering gases at 650 °C, such as methanal, methanol, ethanol, NH_3, NO_2 and so on. The sensor displayed the highest response signal to 20 and 50 ppm acetone compared with the other gases. However, It should not be ignored that the sensor utilizing $Co_{0.5}Zn_{0.5}Fe_2O_4$-SE also showed relative high response to the ethanol and methanol. So, the further work should be done to improve the selectivity to ethanol and methanol.

The surrounding condition causes a great influence on the sensitivity of the sensor, and the water-vapor resistance and stability of the sensor are two decisive factors. So, the responses for the sensor attached with $Co_{0.5}Zn_{0.5}Fe_2O_4$-SE to 50 ppm acetone in the relative humidity (RH) range of 20–98% at 650 °C were measured and the results are shown in Fig. 11(a) and (b), the change amplitudes of the response for the sensor were −3.4% to 4.8%, which indicated the influence of RH on the responses for the sensor was too tiny that can be ignored. Moreover, the stability of the sensor attaching with $Co_{0.5}Zn_{0.5}Fe_2O_4$-SE was explored by continuous test at 650 °C during 40 days. The response of the sensor to 50 and 100 ppm acetone were tested every day and the consequence is exhibited in Fig. 11(c) and Fig. 11(d). The change of the $\Delta V(\Delta V_s)$ to the sensor was in the form of $\Delta Vs = [(\Delta V_n - \Delta V_0)]/\Delta V_0 \times 100\%$, the meanings of ΔV_n and ΔV_0 respectively were the response values of the sensor on the n and initial day, respectively. The changes of response value for the present sensor to 50 and 100 ppm acetone were about −16% and −12% on the 40th day. In addition, the response and recovery curve for the present device to 50 and 100 ppm acetone on the initial, 10th, 20th, 30th and 40th days shown in Fig. 11(d) also further demonstrated the good stability. Thus, the present sensor exhibited good water-vapor resistance and stability during the 40 days test period. Table. 2 records the contrast of the acetone sensing property for the sensor fabricated and widely reported in literature, the present device displayed better sensing properties to acetone than reported devices. The acetone sensing performances, such as sensitivity, low detection limit, water resistance and stability, demonstrated that the sensor had a huge potential prospects in acetone detection.

4. Conclusion

In this work, the mixed potential type electrochemical gas sensors based on YSZ and $Co_{1-x}Zn_xFe_2O_4$ (x = 0, 0.3, 0.5, 0.7 and 1)-SEs with spinel structure synthesized by sol-gel method were developed and used for detection of acetone at 650 °C. The sensor attached with $Co_{0.5}Zn_{0.5}Fe_2O_4$-SE exhibited the largest sensitivity to acetone in the concentration range of 5–100 ppm at 650 °C comparing with those of using other sensing electrode materials. The present sensor also shows the low detection limit of 300 ppb to acetone, which revealed the potential for detection of low concentration acetone. Moreover, the present device also displayed good repeatability, selectivity, humidity resistance, and stability in 40 days work period at high-temperature-aging of 650 °C. Therefore, according to the excellent acetone sensing properties, the present fabricated sensor is considered as a candidate in the aspect of monitoring acetone.

Acknowledgements

This work was supported by the National Nature Science Foundation of China (Nos. 61473132, 61327804, 61474057, 61533021 and 61520106003), The National Key Research and Development Program of China (No.2016YFC0201002), Science and Technology Development Plan of Jilin Province (20140622005JC) and Program for Chang Jiang Scholars and Innovative Research Team in University (No. IRT13018), Application and Basic Research of Jilin Province (2013010 2010JC).

References

[1] D. Dong, M. Shao, Y. Li, S. Lu, Y. Wang, Z. Ji, D. Tang, Carbonyl emissions from heavy-duty diesel vehicle exhaust in China and the contribution to ozone formation potential, J. Environ. Sci. 26 (2014) 122–128.
[2] J. Wang, L. Jin, J. Gao, J. Shi, Y. Zhao, S. Liu, T. Jin, Z. Bai, C. Wu, Investigation of speciated VOC in gasoline vehicular exhaust under ECE and EUDC test cycles, Sci. Total. Environ. 445–446 (2013) 110–116.
[3] X.B. Li, S.Y. Ma, F.M. Li, Y. Chen, Q.Q. Zhang, X.H. Yang, C.Y. Wang, J. Zhu, Porous spheres-like ZnO nanostructure as sensitive gas sensors for acetone detection, Mater. Lett. 100 (2013) 119–123.
[4] L. Wang, A. Teleki, S.E. Pratsinis, P.I. Gouma, Ferroelectric WO_3 nanoparticles for acetone selective detection, Chem. Mater. 20 (2008) 4794–4796.
[5] Z. Jiang, R. Zhao, B. Sun, G. Nie, H. Ji, J. Lei, C. Wang, Highly sensitive acetone sensor based on Eu-doped SnO_2 electrospun nanofibers, Ceram. Int. 42 (2016) 15881–15888.
[6] Q.Q. Jia, H.M. Ji, P. Gao, X. Bai, Z.G. Jin, Control of the acetone sensitive and selective properties of WO_3 nanofibers by doping Co ions: effect of crystal symmetric structure on the responsivity of gas-solid boundaries for gas sensor, J. Mater. Sci. Mater. Electron. 26 (2015) 5792–5802.
[7] F. Liu, X. Yang, B. Wang, Y. Guan, X. Liang, Peng Sun, G. Lu, High performance mixed potential type acetone sensor based on stabilized zirconia and $NiNb_2O_6$ sensing electrode, Sens. Actuators B: Chem. 229 (2016) 200–208.
[8] M. Shnayderman, B. Mansfield, P. Yip, H. Clark, M. Krebs, S. Cohen, J. Zeskind, E. Ryan, H. Dorkin, M. Callahan, T. Stair, J. Gelfand, C. Gill, B. Hitt, C. Davis, Species-specific bacteria identification using differential mobility spectrometry and bioinformatics pattern recognition, Anal. Chem. 77 (2005) 5930–5937.
[9] S. Choi, W. Ryu, S. Kim, H. Cho, I. Kim, Bi-functional co-sensitization of graphene oxide sheets and Ir nanoparticles on p-type Co_3O_4 nanofibers for selective acetone detection, J. Mater. Chem. B 2 (2014) 7160–7167.
[10] L. Wang, A. Teleki, S. Pratsinis, P. Gouma, Ferroelectric WO_3 nanoparticles for acetone selective detection, Chem. Mater 20 (2008) 4794–4796.
[11] P. Sun, Y. Cai, S. Du, X. Xu, L. You, J. Ma, F. Liu, X. Liang, Y. Sun, G. Lu, Hierarchical α-Fe_2O_3/SnO_2 semiconductor composites: hydrothermal synthesis and gas sensing properties, Sens. Actuators B: Chem. 182 (2013) 336–343.
[12] X. Zhou, J. Liu, C. Wang, P. Sun, X. Hu, X. Li, K. Shimanoe, N. Yamazoe, G. Lu, Highly sensitive acetone gas sensor based on porous $ZnFe_2O_4$ nanospheres, Sens. Actuators B: Chem. 206 (2015) 577–583.
[13] J. Zosel, K. Ahlborn, R. Müller, D. Westphal, V. Vashook, U. Guth, Selectivity of HC-sensitive electrode materials for mixed potential gas sensors, Solid State Ionics 169 (2004) 115–119.
[14] L. Tang, Y. Li, K. Xu, X. Hou, Y. Lv, Selective acetone sensor based on its cataluminescence from nano-La_2O_3 surface, Sens. Actuators B: Chem. 132 (2008) 243–249.
[15] T. Nasution, I. Nainggolan, S. Hutagalung, K. Ahmad, Z. Ahmad, The sensing mechanism and detection of low concentration acetone using chitosan-based sensor, Sens. Actuators B: Chem. 177 (2013) 522–528.
[16] M. Mori, H. Nishimura, Y. Itagaki, Y. Sadaoka, Potentiometric VOC detection in air using 8YSZ-based oxygen sensor modified with $SmFeO_3$ catalytic layer, Sens. Actuators B: Chem. 142 (2009) 141–146.
[17] T. Xiao, X. Wang, Z. Zhao, L. Li, L. Zhang, H. Yao, J. Wang, Z. Li, Highly sensitive and selective acetone sensor based on C-doped WO_3 for potential diagnosis of diabetes mellitus, Sens. Actuators B: Chem. 199 (2014) 210–219.
[18] H. Zhang, C. Yin, Y. Guan, X. Cheng, X. Liang, G. Lu, NASICON-based acetone sensor using three-dimensional three-phase boundary and Cr-based spinel oxide sensing electrode, Solid State Ionics 262 (2014) 283–287.
[19] M. Kasalizadeh, A. Khodadadi, Y. Mortazavi, Coupled metal oxide-doped Pt/SnO_2 semiconductor and yittria-stabilized zirconia electrochemical sensors for detection of VOCs, J. Electrochem. Soc. 160 (2013) B218–B224.
[20] F. Liu, Y. Guan, R. Sun, X. Liang, P. Sun, F. Liu, G. Lu, Mixed potential type acetone sensor using stabilized zirconia and $M_3V_2O_8$ (M: Zn Co and Ni) sensing electrode, Sens. Actuators B: Chem. 221 (2015) 673–680.
[21] Q. Diao, C. Yin, Y. Guan, X. Liang, S. Wang, Y. Liu, Y. Hu, H. Chen, G. Lu, The effects of sintering temperature of $MnCr_2O_4$ nanocomposite on the NO_2 sensing property for YSZ-based potentiometric sensor, Sens. Actuators B: Chem. 177 (2013) 397–403.
[22] N. Ueda, T. Omata, N. Hikuma, K. Ueda, H. Mizoguchi, T. Hasimoto, H. Kawazoe, T. Hashimoto, Appl. Phys. Lett. 61 (1992) 1954.
[23] T. Omata, N. Ueda, N. Hikuma, K. Ueda, H. Mizoguchi, T. Hashimoto, H. Kawazoe, Appl. Phys. Lett. 62 (1993) 499.
[24] T. Omat, N. Ueda, K. Ueda, H. Kawazoe, Appl. Phys. Lett. 64 (1994) 1077.
[25] E.L. Brosha, R. Mukundan, R. Lujan, F.H. Garzon, Mixed potential NO_x sensors using thin film electrodes and electrolytes for stationary reciprocating engine type applications, Sens. Actuators B: Chem. 119 (2006) 398–408.
[26] H. Deligoz, A. Baykal, M.S. Toprak, E.E. Tanriverdi, Z. Durmusb, H. Sozerif, Synthesis structural, magnetic and electrical properties of $Co_{1-x}Zn_xFe_2O_4$ (x = 0.0, 0.2) nanoparticles, Mater. Res. Bull. 48 (2013) 646–654.
[27] R. Rani, G. Kumar, K.M. Batoo, M. Singh, Influence of temperature on the electric, dielectric and AC conductivity properties of nano-crystalline zinc

substituted cobalt ferrite synthesized by solution combustion technique, Appl. Phys. A 115 (2014) 1401–14407.
[28] C. Wang, X. Cheng, X. Zhou, P. Sun, X. Hu, K. Shimanoe, G. Lu, N. Yamazoe, Hierarchical α-Fe_2O_3/NiO composites with a hollow structure for a gas sensor, ACS Appl. Mater. Interfaces 6 (2014) 12031–12037.
[29] H. Fan, Y. Zeng, H. Yang, X. Zheng, L. Liu, T. Zhang, Preparation and gassensitive properties of ZnO-CuO nanocomposites, Acta Phys. Chem. Sin. 24 (2008) 1292–1296.
[30] P. Sun, X. Zhou, C. Wang, B. Wang, X. Xu, G. Lu, One-step synthesis and gas sensing properties of hierarchical Cd-doped SnO_2 nanostructures, Sens. Actuators B: Chem. 190 (2014) 32–39.
[31] G. Lu, N. Miura, N. Yamazoe, High-temperature sensors for NO and NO_2 based on stabilized zirconia and spinel-type oxide electrodes, J. Mater. Chem. 7 (1997) 1445–1449.
[32] N. Miura, J. Wang, M. Nakatou, P. Elumalai, S. Zhuiykov, M. Hasei, High-temperature operating characteristics of mixed-potential-type NO_2 sensor based on stabilized-zirconia tube and NiO sensing electrode, Sens. Actuators B: Chem. 114 (2006) 903–909.
[33] Q. Diao, C. Yin, Y. Liu, J. Li, X. Gong, X. Liang, S. Yang, H. Chen, G. Lu, Mixed-potential-type NO_2 sensor using stabilized zirconia and Cr_2O_3-WO_3 nanocomposites, Sens. Actuators B: Chem. 180 (2013) 90–95.
[34] V. Plashnitsa, T. Ueda, N. Miura, Improvement of NO_2 a sensing performances by an additional second component to the nano-structured NiO sensing electrode of a YSZ-based mixed-potential type sensor, Int. J. Appl. Ceram. Technol. 3 (2006) 127–133.
[35] N. Miura, T. Sato, S. Anggraini, H. Ikeda, S. Zhuiykov, A review of mixed-potential type zirconia-based gas sensors, Ionics 20 (2014) 901–925.
[36] H. Zhang, T. Zhong, R. Sun, X. Liang, G. Lu, Sub-ppm H_2S sensor based on NASICON and $CoCr_{2-x}Mn_xO_4$ sensing electrode, RSC Adv. 4 (2014) 55334–55340.
[37] N. Miura, M. Nakatou, S. Zhuiykov, Impedancemetric gas sensor based on zirconia solid electrolyte and oxide sensing electrode for detecting total NO_x at high temperature, Sens. Actuators B: Chem. 93 (2003) 221–228.
[38] M. Nakatou, N. Miura, Detection of propene by using new-type impedancemetric zirconia-based sensor attached with oxide sensing-electrode, Sens. Actuators B: Chem. 120 (2006) 57–62.
[39] Y. Chen, J.Z. Xiao, Effects of YSZ addition on the response of La_2CuO_4 sensing electrode for a potentiometric NO_x sensor, Sens. Actuators B: Chem. 192 (2014) 730–736.
[40] P.K. Sekhar, K. Subramaniyam, Electrical characterization of a mixed potential propylene sensor, Sens. Actuators B: Chem. 188 (2013) 367–371.
[41] N. Miura, H. Kurosawa, M. Hasei, G. Lu, N. Yamazoea, Stabilized zirconia-based sensor using oxide electrode for detection of NO_x in high-temperature combustion-exhausts, Solid State Ionics 86–88 (1996) 1069–1073.
[42] N. Miura, G. Lu, N. Yamazoe, Progress in mixed-potential type devices based on solid electrolyte for sensing redox gases, Solid State Ionics 136–137 (2000) 533–542.
[43] P. Elumalai, J. Wang, S. Zhuiykov, D. Terada, M. Hasei, N. Miura, Sensing characteristics of YSZ-based mixed-potential-type planar NO_x sensors using NiO sensing electrodes sintered at different temperatures, J. Electrochem. Soc. 152 (2005) H95–H101.
[44] G. Lu, Q. Diao, C. Yin, S. Yang, Y. Guan, X. Cheng, X. Liang, High performance mixed-potential type NO_x sensor based on stabilized zirconia and oxide electrode, Solid State Ionics 262 (2014) 292–297.
[45] B. Wang, F. Liu, X. Yang, Y. Guan, C. Ma, X. Hao, X. Liang, F. Liu, P. Sun, T. Zhang, G. Lu, Fabrication of Well-Ordered Three-Phase Boundary with Nanostructure Pore Array for Mixed Potential-Type Zirconia-Based NO_2 Sensor, ACS Appl. Mater. Interfaces 8 (2016) 16752–16760.
[46] H. Zhang, C. Yin, Y. Guan, X. Cheng, X. Liang, G. Lu, NASICON-based acetone sensor using three-dimensional three-phase boundary and Cr-based spinel oxide sensing electrode, Solid State Ionics 262 (2014) 283–287.
[47] M. Kasalizadeh, A. Khodadadi, Y. Mortazavi, Coupled metal oxide-doped Pt/SnO_2 semiconductor and yittria-stabilized zirconia electrochemical sensors for detection of VOCs, J. Electrochem. Soc. 160 (2013) B218–B224.
[48] X. Zhou, W. Feng, C. Wang, X. Hu, X. Li, P. Sun, K. Shimanoe, N. Yanazoe, G. Lu, Porous ZnO/$ZnCr_2O_4$ hollow spheres: synthesis, characterization, and applications in gas sensing, J. Mater. Chem. A 2 (2014) 17683–17690.
[49] J. Huang, X. Xu, C. Gu, M. Yang, M. Yang, J. Liu, Large-scale synthesis of hydrated tungsten oxide 3D architectures by a simple chemical solution route and their gas-sensing properties, J. Mater. Chem. 21 (2011) 13283–13289.
[50] P. Song, Q. Wang, Z. Yang, Preparation, characterization and acetone sensing properties of Ce-doped SnO_2 hollow spheres, Sens. Actuators B: Chem. 173 (2012) 839–846.
[51] Y. Zeng, T. Zhang, M. Yuan, M. Kang, G. Lu, R. Wang, H. Fan, Y. He, H. Yang, Growth and selective acetone detection based on ZnO nanorod arrays, Sens. Actuators B: Chem. 143 (2009) 93–98.
[52] X. Zhou, X. Li, H. Sun, P. Sun, X. Liang, F. Liu, X. Hu, G. Lu, Nanosheet-assembled $ZnFe_2O_4$ hollow microspheres for high-sensitive acetone sensor, ACS Appl. Mater. Interfaces 7 (2015) 15414–15421.
[53] X. Li, C. Wang, H. Guo, P. Sun, F. Liu, X. Liang, G. Lu, Double-shell architectures of $ZnFe_2O_4$ nanosheets on ZnO hollow spheres for high- performance gas sensors, ACS Appl. Mater. Interfaces 7 (2015) 17811–17818.

Biographies

Xidong Hao received the B.Eng. degree in department of electronic science and technology in 2016. He is currently studying for his M.E. Sci. degree in College of Electronic Science and Engineering, Jilin University, China.

Bin Wang received the B.Eng. degree in department of electronic science and technology in 2015. He is currently studying for his M.E. Sci. degree in College of Electronic Science and Engineering, Jilin University, China.

Ce Ma received the B.Eng. degree in department of electronic science and technology in 2016. He is currently studying for his M.E. Sci. degree in College of Electronic Science and Engineering, Jilin University, China.

Fangmeng Liu received his B.S. degree in 2009 from College of Chemistry, Liaocheng University and M.S. degree in 2012 from Northeast Forestry University in China. Currently he is studying for his Ph.D. degree in College of Electronic Science and Engineering, Jilin University, China.

Xue Yang received the B.Eng. degree in department of electronic science and technology in 2015. She is currently studying for his M.E. Sci. degree in College of Electronic Science and Engineering, Jilin University, China.

Tong Liu received the B.Eng. degree in department of electronic science and technology in 2015. She is currently studying for his M.E. Sci. degree in College of Electronic Science and Engineering, Jilin University, China.

Xishuang Liang received the B. Eng. degree in Department of Electronic Science and Technology in 2004. He received his Doctor's degree in College of Electronic Science and Engineering at Jilin University in 2009. Now he is an associate professor of Jilin University, China. His current research is solid electrolyte gas sensor.

Chunhua Yang is a professor and works in School of Information Science and Engineering, Central South University, China. Her research interests are focused on automation and computer control.

Hongqiu Zhu is an associate professor and works in School of Information Science and Engineering, Central South University, China. His research interests are focused on automation and computer control.

Geyu Lu received the B.Sci. degree in electronic sciences in 1985 and the M.S.degree in 1988 from Jilin University in China and the Dr. Eng. degree in 1998 from Kyushu University in Japan. Now he is a professor of Jilin University, China. His current research interests include the development of chemical sensors and the application of the function materials.